

# Phase diagram of the Cairo pentagonal XXZ spin-1/2 magnet under a magnetic field

Arnaud Ralko

Institut Néel, UPR2940, CNRS et Université de Grenoble, Grenoble, FR-38042 France

(Dated: August 15, 2021)

The phase diagram of the XXZ spin-1/2 magnet, equivalent to hard-core bosons, under a staggered magnetic field and on the *Cairo* pentagonal lattice is computed at zero and finite temperature by using a cluster mean field theory and a stochastic series expansion quantum Monte Carlo. The complex connectivity and the frustration lead to unconventional phases such as a 1/3-ferrimagnetic plateau stabilized by quantum fluctuations as well as a 5/12-topological phase induced by a local ice-rule constraint. We also report the presence of a ferrimagnetic superfluid and its thermal melting. Finally, we discuss the ferro- and antiferro- magnetic (hopping sign) cases.

These last years, important discoveries in strongly correlated physics have been reported in systems where frustration plays a central role. Geometrical frustration is very interesting in that respect. A large variety of unusual phases is encountered, from (insulating) exotic spin liquids<sup>1-3</sup> to superconductivity<sup>4</sup>. Recent developments on frustrated *optical lattices* of cold atoms open new directions for stabilizing exotic bosonic phases such as supersolids<sup>5</sup> or Bose-metals<sup>6-8</sup>.

A case of interest is that of *ice-rule* systems for which highly degenerate classical ground states (GS) are governed by a local constraint<sup>9</sup>. For spin-1/2 (boson), it corresponds to a fixed number of up (occupied) and down (empty) spins (sites) on each elementary brick: a tetrahedron on pyrochlore and checkerboard lattices<sup>10,11</sup> or a triangle on the kagome<sup>12</sup>. They provide striking features such as charge fractionalization<sup>13</sup>, Coulomb-gas phases and even *magnetic monopoles*<sup>14</sup>. Their quantum melting is of broad interest but remains a highly non-trivial question; aside from the strength of the interactions, the lattice geometry can play a relevant role. Some works in this direction revealed exotic phases, *e.g.* a commensurate *Resonating Valence Bond* supersolid on the checkerboard lattice<sup>15</sup>. Hence, it is natural to search for ice-rule systems with more complex geometries such as inequivalent site lattices<sup>16</sup>.

Recently, Ressouche *et al.* rendered accessible the two dimensional *Cairo* pentagonal structure to experiments by proposing the iron-based compound  $\text{Bi}_2\text{Fe}_4\text{O}_9$ <sup>17</sup>. So far it is the only known compound with such geometry, a spin-5/2 antiferromagnet made of identical non-regular pentagons with a site dependent connectivity  $c_i$  of 3 ( $z_3$  site) and 4 ( $z_4$  site) neighbors as depicted in Fig.1-a. Note that this *Cairo* lattice is the dual of the Shastry-Sutherland lattice for which the GS could be a spin-liquid<sup>19</sup>. From the quantum side, substituting the iron atoms by copper ones in the  $\text{Bi}_2\text{Fe}_4\text{O}_9$ <sup>18</sup>, or creating complex optical lattices, the square-based *cairo* lattice for example (Fig.1-b), is undoubtedly a major challenge. However, in view of the recent original phases reported in frustrated systems<sup>20-22</sup>, inequivalent-site structures possess all the ingredients to expect unconventional physics.

In this paper, we study a spin-1/2 magnet under a staggered magnetic field, or equivalently the extended hard-core boson Hubbard model, on the *Cairo* pentagonal lattice. We report a rich phase diagram obtained both at zero and at low temperature. We focus on the different insulating phases: a *topological* ice-rule of two bosons per pentagon, a 2/3-checkerboard and a pure quantum 1/3-ferrimagnetic phase with no local constraint. Moreover, a large region of ferrimag-

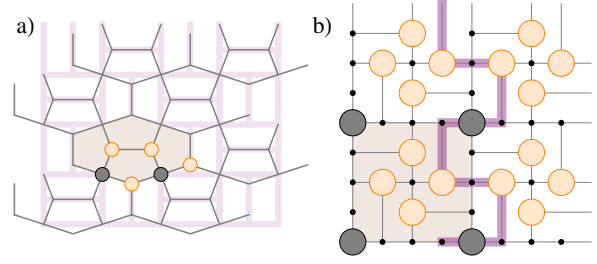


FIG. 1: (Color online). a) The *Cairo* pentagonal lattice and its 6-site unit-cell (shaded plaquette) containing 2  $z_4$  sites (dark points) and 4  $z_3$  sites (light points). The continuously deformed square-based *Cairo* lattice used in this work is displayed in the background. b) One of the authorized 5/12 topological *ice-rule* configurations with two spins up (bosons) per pentagon (disks). Thick line: typical *winding-loop* along which a shift of all encountered bosons of one lattice site preserves the ice-rule constraint. Shaded plaquette: the 12-site cluster (2 unit-cells) used in the CMFT.

netic superfluid is identified as well as its Kosterlitz-Thouless (KT) transition<sup>23</sup> at strong repulsion induced by thermal fluctuations. We also compare the ferro- and antiferro- magnetic cases (sign of the hopping) and discuss the case of the uniform magnetic field (nature of the chemical potential).

## I. MODEL AND METHODS

Spin-1/2 on the pentagonal lattice can be described by an extended hard-core boson Hubbard model, with a repulsive nearest neighbor interaction  $V$ , a hopping  $t$  and a chemical potential  $\mu_i$ , given by:

$$\mathcal{H} = -t \sum_{\langle i,j \rangle} (b_i^\dagger b_j + h.c.) + V \sum_{\langle i,j \rangle} n_i n_j - \sum_i \mu_i n_i \quad (1)$$

where  $i$  is the site index,  $b_i^\dagger$  is the creation operator and  $n_i$  the number of bosons. The correspondence is done by the mapping  $S_i^\dagger = b_i^\dagger$  and  $S_i^z = n_i - 1/2$  and Eq.(1) is equivalent to a XXZ spin-1/2 magnet with spin couplings  $J_z = V$  and  $J_\perp = -2t$ , under an effective magnetic field  $h_i$ . The chemical potential  $\mu_i$  is an adjustable parameter<sup>20</sup>; this leads to two important cases for systems with anisotropic  $c_i$ , it can be either (a) site dependent or (b) constant. In case (a), if  $\mu_i$  is set to  $\mu + c_i V/2$ , we have the well-known spin-1/2 magnet under

a uniform magnetic field<sup>24</sup>. In case (b), the system experiences a staggered magnetic field  $h_i = \mu - c_i V/2$  depending explicitly on the connectivity. Experimentally, this can occur in systems with alternating crystal structure and the possible presence of a Dzyaloshinskii-Moriya interaction<sup>25</sup>. These two cases are of great importance in quantum magnetism, but the latter case can obviously provide unexpected behaviors as has been recently shown in 1D materials<sup>26</sup>. In the present work, we hence focus on constant  $\mu$  and draw out the rich phase diagram induced by the complex connectivity  $c_i$ . We use equivalently bosonic or spin language when appropriate.

To simplify the analysis, we map the parameters on a sphere described by two angles  $\theta$  and  $\phi$  in such a way that  $\bar{\mu} = \sin \phi$ ,  $\bar{t} = \cos \theta \cos \phi$  and  $\bar{V} = \sin \theta \cos \phi$ , where  $(\bar{t}, \bar{V}, \bar{\mu})$  are dimensionless. We also consider a deformed *square-based* version of the original lattice, see Fig.1-b. The phase diagram

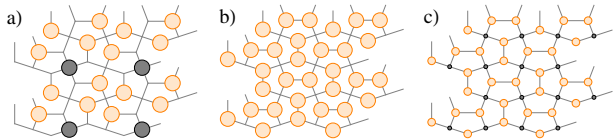


FIG. 2: (Color online). Schematic representation of the insulating phases of Fig.3. Dark (light) circles stand for  $z_4$  ( $z_3$ ) sites and the size is proportional to the magnetization (boson density). (a) A typical 5/12-topological ice-rule configuration, (b) the 2/3-checkerboard and (c) the quantum 1/3-ferrimagnetic.

(Fig.3) is obtained by using two numerical methods: a Cluster Mean Field Theory (CMFT)<sup>27</sup> and a Stochastic Series Expansion (SSE) Quantum Monte-Carlo (QMC)<sup>28</sup> at respectively zero and finite temperature. The basis of the CMFT is to consider a finite cluster for which internal bonds of Eq. (1) are treated exactly whereas the boundary conditions are coupled to an external bath. Here, we use a 12-site cluster shown in Fig.1-b (shaded region) and corresponding to two unit-cells. The system is diagonalized and solved self-consistently. Note that for the triangular lattice, this method gives an excellent agreement with the QMC results<sup>29</sup>. Here, it also allows us to consider the frustrated  $t < 0$  case (antiferromagnet) in addition to the  $T=0$  properties. The SSE algorithm provides unbiased quantum simulations for very large system sizes, in our case  $N = l\sqrt{3}/4 \times l\sqrt{3}/4$  with  $l$  up to 72 (3888 sites), and at finite temperature  $T$ . Usually,  $T^{-1} = 2l$  is enough to focus on GS properties<sup>30,31</sup>. At very large repulsion however, the Kosterlitz-Thouless temperature  $T_{KT}$  significantly drops down and a finite temperature transition at small  $T$  is expected. In this work, the phase diagram is computed at  $T^{-1} = 100 > 2l$  (up to  $l = 48$ ) and thermal effects are considered.

We consider four quantities:  $x$  the average number of bosons (spin magnetization),  $\rho_S$  the superfluid density (spin stiffness) implemented via the winding numbers in the SSE<sup>28</sup>,  $p_n$  the average number of pentagons with exactly  $n$  up-spins and the order parameter  $M^2(\mathbf{q}) = \langle \psi_0 | n(-\mathbf{q}) n(\mathbf{q}) | \psi_0 \rangle / N$  with  $n(\mathbf{q}) = \sum_i e^{i\mathbf{q}\cdot\mathbf{r}_i} n_i$  performed separately on all sites of the non-Bravais square-based lattice at  $\mathbf{q} = (\pi, \pi)$  ( $M_{\text{all}}$ ) and on the  $z_i$  sublattice at  $\mathbf{q} = (0, 0)$  ( $M_{z_i}$ )<sup>31,32</sup>. The square-based

Cairo lattice being a depleted square lattice with extra bonds (*longer* bonds on Fig.1-b), a finite  $M(\mathbf{q})$  is expected even for a disordered phase, as entirely explained in [31].

## II. OVERVIEW OF THE PHASE DIAGRAM

In Fig.3 are depicted the zero (CMFT - dashed lines) and finite (SSE - symbols) temperature phase diagrams in the large repulsion limit  $\theta/\pi > 0.3$  where insulating phases appear. To characterize the different phases, we have considered two cut lines respectively at fixed  $\theta$  and  $\phi$  shown in Fig.3. Since the phase diagram is very rich, we briefly introduce it in this paragraph before giving more details in the rest of the paper. Close to  $\theta = \pi/2$  ( $V/t \rightarrow \infty$ ), only reachable by the mean-field, the frustration leads to two magnetization plateaus at  $x = 2/3$  and  $5/12$  (see Fig.2) at  $T = 0$ . Surprisingly, when quantum fluctuations are turned on ( $\theta < \pi/2$ ) a third insulating plateau at  $x = 1/3$  arises. This insulator is not stabilized at the classical limit, is fully driven by the quantum fluctuations and stabilized by the frustration ( $t < 0$ ). The quantum melting of these lobes leads, in spin language, to a *ferrimagnetic* superfluid (SF) corresponding to different magnetizations (boson density) on each sublattice. Uncompensated phases have already been reported in systems with complex coordination<sup>16</sup>. The

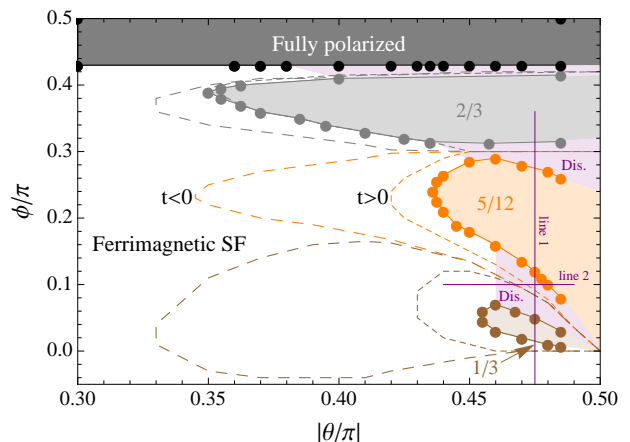


FIG. 3: (Color online). Phase diagram in the  $(\theta, \phi)$  plane and the comparison between zero (CMFT, dashed lines) and finite (SSE for  $\theta/\pi < 0.485$ , symbols) temperature. Insulating phases (lobes) are enhanced at zero temperature and by frustration ( $t < 0$ ). The ferrimagnetic superfluid (SF) has a Kosterlitz-Thouless (KT) transition to a disordered region (Dis.) at finite  $T$ . Lines 1 and 2 are the scans used respectively in Fig.4 and Fig.5.

finite  $T$  phase diagram is computed via the SSE method up to  $\theta/\pi = 0.485$  (circles in Fig.3). Stronger interaction results (shaded regions) are extrapolated. The main difference with the  $T = 0$  case is the presence of disordered regions (Dis.) due to thermal fluctuations, a Kosterlitz-Thouless transition of the SF phases and/or the melting of the insulating lobes. Note that small discrepancies between the methods cannot be avoided. In the following, we detail the phases of Fig.3. In particular, we describe the ferrimagnetic character of the SF

phase and provide a temperature analysis at strong interaction before presenting the unconventional insulators.

### III. SUPERFLUIDITY AND THERMAL FLUCTUATIONS

As mentioned above, at zero  $T$  and for  $\theta$  small enough, the system is a superfluid ( $\rho_S \neq 0$ ) with an on-site magnetization (boson density) depending on the connectivity  $c_i$ . We refer to this phase as the *ferrimagnetic* SF<sup>24</sup>. We have computed the four physical quantities following two cut-lines depicted in Fig.3 at both fixed  $\theta$  (line 1, Fig.4) and  $\phi$  (line 2, Fig.5). On Fig.4 are displayed from the top to the bottom  $x$ ,  $\rho_S$ ,  $M^2(q)$  and  $p_n$ , as a function of  $\phi$  and at finite  $T$ . More information

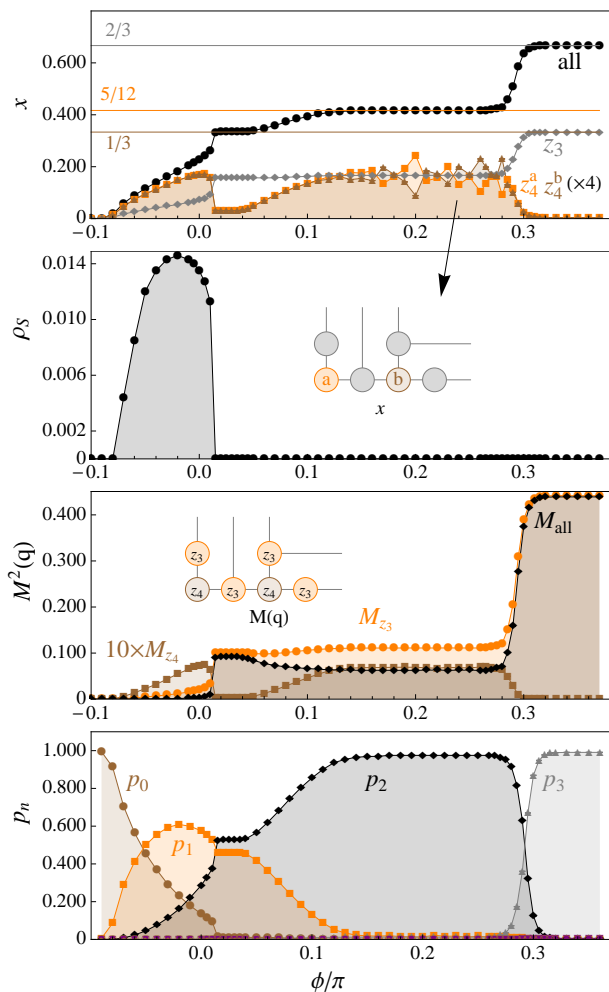


FIG. 4: (Color online). Scan along the line 1 of Fig.3 at strong repulsion ( $\theta = 0.475\pi$ ), for the cluster size  $l = 40$  and at finite  $T$ . From top to bottom: the magnetization  $x$  (boson density); the spin stiffness  $\rho_S$  (superfluid density); the order parameter  $M^2(q)$  at  $(\pi, \pi)$  for  $M_{\text{all}}$  (all sites) and  $(0, 0)$  for  $M_{z_i}$  ( $z_i$  sublattice); the average number of pentagons  $p_n$  with  $n$  up spins (bosons). Inset: sublattices used for  $x$  and  $M^2(q)$  indicated by arrows.

can be obtained by computing  $x$  and  $M(q)$  on the sublattices  $z_3$  and  $z_4$  as well. For  $\phi < 0.2\pi$ ,  $x_{z_3} \neq x_{z_4}$  while  $\rho_S \neq 0$

hence corroborating the presence of the ferrimagnetic SF. At  $T = 0$  and for  $\theta$  large enough ( $> 0.45\pi$ ), either transitions of first order between two lobes or second order with a superfluid are observed (reinforced at  $t < 0$ ). At finite  $T$  (SSE), disordered regions (Dis. in Fig.3) with a finite compressibility  $dx/d\phi \neq 0$  and  $\rho_S = 0$  emerge, related to a Kosterlitz-Thouless (KT) transition; a finite  $\rho_S$  (broken U(1) symmetry) in 2D is indeed allowed up to a  $T_{\text{KT}}$  temperature. In Fig.5 is depicted the size-scaling up to  $l = 72$  (upper panel) and the  $T$  dependence (lower panel) of  $\rho_S$  for  $\phi = 0.1\pi$  (line 2). From

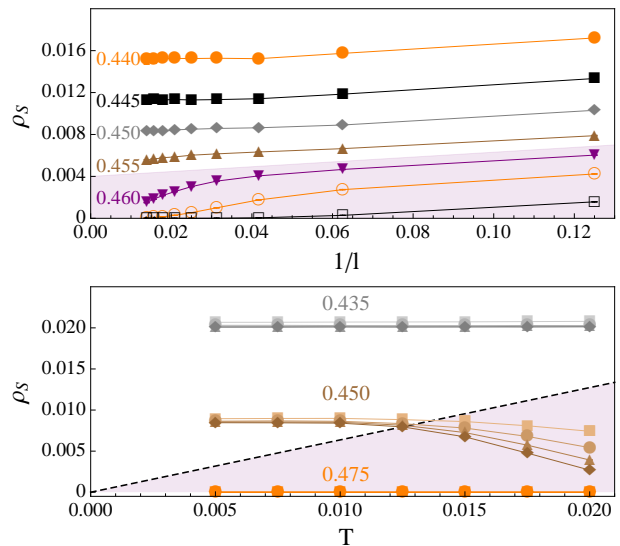


FIG. 5: (Color online). Scan along the line 2 of Fig.3 at  $\phi/\pi = 0.1$  of  $\rho_S$  as a function of the size  $l$  at  $T = 0.01$  (upper) and as a function of the  $T$  for sizes up to  $l = 16, 24, 32$  and  $40$  (lower, symbols). The dashed line is the  $2T/\pi$  line for which a crossing with  $\rho_S(T)$  indicates the Kosterlitz-Thouless transition. Shadings: disordered phases of Fig.3.

the upper panel, a transition between  $\rho = 0$  and  $\neq 0$  occurs at the thermodynamic limit (TDL). For 2D systems, the KT transition is located by the universal jump at  $\rho_S(T_{\text{KT}}) = 2T_{\text{KT}}/\pi$  plus some logarithmic finite size corrections<sup>30</sup>. This is calculated in Fig.5 for 3 representative values of  $\theta/\pi$  along line 2: (i) deep in the SF phase (0.435), (ii) close to the transition (0.45) and (iii) in the  $\rho_S = 0$  region (0.475). We obtain (i)  $T < T_{\text{KT}}$ , (ii)  $T_{\text{KT}} \simeq 0.0125$  close to  $T$  and (iii)  $T_{\text{KT}} \ll T$  with a KT transition at  $\theta/\pi \simeq 0.46$ . The finiteness of  $T_{\text{KT}}$  is non-trivial and beyond the scope of this paper. However, it is related to the propagation of defects while doping an insulator. For example, adding a boson in the  $5/12$  ice-rule phase results in creating two  $p_3$  defects with zero energy dynamics. This would be compatible with a small but finite  $T_{\text{KT}}$  at the TDL.

### IV. THE INCOMPRESSIBLE PHASES

*The 2/3-checkerboard phase* – On Fig.4, at  $\phi/\pi > 0.3$ , all the pentagons carry 3 bosons ( $p_3 = 1$ ),  $\rho_S = 0$  and  $M(q)$  is finite for the  $z_3$  sublattice while zero on the  $z_4$  sites. This is in

agreement with filled  $x_{z_4}$  sites and empty  $x_{z_3}$ . This order is a simple checkerboard crystal (Fig.2-b) and is the largest lobe of Fig.3, with  $\theta_{\max} \simeq 0.35\pi$  at  $\phi \simeq 0.39\pi$  since adding one particle costs the energy  $4V$ . All the  $z_3$  sites are up spins.

*The 1/3-ferrimagnetic phase* – The 1/3 plateau is one of the unexpected phases obtained in this geometry which arises only under quantum fluctuations (see Fig.3), both at zero and finite  $T$ . It is stabilized either under a staggered or a constant<sup>24</sup> magnetic field and its expansion is 10 times larger (in unit of  $V/t$ ) for  $t < 0$ . It is insulating ( $\rho_s = 0$ ) with no ice-rule constraint ( $p_{1,2} \neq 0$ , Fig.4) and no broken lattice symmetry<sup>32</sup>. The internal unit cell densities  $x_{z_3}$  and  $x_{z_4}$  mismatch (Fig.4) showing a ferrimagnetic character at magnetization 1/3 (Fig.2-c). As displayed in Fig.4 at finite  $T$ , the 1/3 phase is surrounded by two phase transitions, a first order with the SF for  $\phi/\pi \simeq 0.01$  and a continuous transition with the disordered phase. At  $T = 0$  however, the disordered phase is not present and a first order transition between the 1/3 phase to the 5/12 one is obtained (dashed lines in Fig.3). The tip of the 1/3 lobe in Fig.3 is located at  $\theta/\pi \simeq 0.455$  precisely where the first order transition vanishes.

*The topological ice-rule phase* – The 5/12 plateau is stabilized when the magnetic field is staggered (constant  $\mu_i$ ). Stable at the Ising limit (CMFT), this phase is robust against both quantum and thermal fluctuations, specifically at  $t < 0$  (Fig.3). On Fig.4,  $\rho_s = 0$  and an average of 2 bosons on  $z_3$  sites against 0.5 on  $z_4$  ones per unit-cell is observed.  $M(q)$  is larger than the depletion induced internal structure signal, indicating a clear difference between the sublattices<sup>31,32</sup>. With  $p_2 = 1$ , we deduce the presence of an *ice-rule* of two bosons per pentagon. A typical configuration of this 5/12 phase is given in Fig.2-a. By labelling the  $z_4$  sites inside a unit-cell as  $z_4^a$  and  $z_4^b$  (inset of Fig.4), we identify a finite distribution of  $x_{z_4^a}$  and  $x_{z_4^b}$  w.r.t.  $\phi$  related to the degeneracy of the GS. Classical zero-energy configurations in standard ice-rule systems can generally be connected by quantum tunneling of a finite number of particles on a closed path. This leads, through perturbation theory, to a quantum effective Hamiltonian *e.g.* quantum dimer models (QDM)<sup>15,33,34</sup> or loop models<sup>13,35</sup>. Here, no such local moves are available, only *winding-loops* invoking the boundary conditions instead (see Fig.1-b). Bosons on such a loop have only two possible positions that respect the ice-rule constraint and a tunneling from one to the other results in a new 5/12 configuration. For a cluster of size  $l$ , there are  $l/4$  distinct con-

tours in each direction ( $x$  and  $y$ ). For a given configuration, the number of bosons on such a contour is a conserved quantity and each set of these quantities defines a topological sector. Only the global shift of the bosons along a winding-loop can change this number and thus the topological sector; the system is protected from local disorder. Starting from the most symmetrical 5/12 configuration (Fig.1-b), the total number of winding loops is  $l/2$ . A shift of the bosons along one direction cancels the possible winding-loops along the other. The number of connected configurations is then simply  $\Omega = 2 \times 2^{l/4}$ . The zero-temperature entropy per site hence scales as  $S/N = \frac{(l+4)\log 2}{3l^2}$  and vanishes at the  $l \rightarrow \infty$  limit. Since all the configurations are frozen, the phase transition is not smooth, as confirmed by the sudden appearance of the distribution. We estimate the width of the 5/12 plateau by the expansion of this distribution, *e.g.*  $0.13(1) \leq \phi/\pi \leq 0.26(1)$  in Fig.4. To our knowledge, isolated sectors have always been reported in systems where local moves were also available<sup>33</sup>.

## V. CONCLUDING REMARKS

We report the phase diagram of spin-1/2 magnets (hard core bosons) on the *Cairo* pentagonal lattice, at zero (CMFT) and finite (SSE) temperature. The anisotropic connectivity leads, at constant  $\mu_i$ , to a staggered magnetic field<sup>25,26</sup>. Various insulating phases are identified among which a pure quantum induced 1/3-ferrimagnetic phase, not stabilized in the Ising limit ( $\theta = \pi/2$ )<sup>24</sup>. An original 5/12-topological ice-rule phase is evidenced, emphasizing the main difference between spin-1/2 systems under staggered and uniform fields. In this system, the effect of the frustration ( $t < 0$ ) enhances the insulating phases. Finally, a zero *vs.* finite  $T$  comparison reveals a KT transition located at strong repulsion as well as a partial melting of the lobes. The two methods employed here are in good agreement. Open issues remain, such as the complete description of the phase transitions and the temperature properties. Nevertheless, the spin-1/2 Cairo magnet is a very promising candidate for exploring new states of matter.

*Acknowledgements* – I thank O. Cépas and V. Simonet for discussions. I am indebted to A. Läuchli and D. Poilblanc for valuable critical comments of the manuscript. I am also grateful to N. Dempsey for the careful rereading of this manuscript.

<sup>1</sup> P. Mendels, F. Bert, M. A. de Vries, A. Olariu, A. Harrison, F. Duc, J. C. Trombe, J. S. Lord, A. Amato, and C. Baines, *Phys. Rev. Lett.* **98**, 077204 (2007).  
<sup>2</sup> F. Mila, F. Vernay, A. Ralko, F. Becca, P. Fazekas, and K. Penc, *J. Phys. Cond. Matt.* **19** 145201 (2007); A. Ralko, M. Ferrero, F. Becca, D. Ivanov, and F. Mila, *Phys. Rev. B* **76**, 140404(R) (2007).  
<sup>3</sup> Y. Ran, M. Hermele, P. A. Lee, and X.-G. Wen, *Phys. Rev. Lett.* **98**, 117205 (2007).  
<sup>4</sup> D. C. Johnston, *J. of Low Temp. Phys.* **25**, 145 (1976).  
<sup>5</sup> J. Ruostekoski, *Phys. Rev. Lett.* **103**, 080406 (2009).

<sup>6</sup> M. V. Feigelman and V. B. Geshkenbein, *Phys. Rev. B* **48** 16641 (1993).  
<sup>7</sup> D. Das and S. Doniach, *Phys. Rev. B* **60** 1261 (1999).  
<sup>8</sup> A. Paramekanti, L. Balents, and M. P. A. Fisher, *Phys. Rev. B* **66** 054526 (2002).  
<sup>9</sup> Ice-rules bring novel features w.r.t. the bandwidth-controlled Mott transition at half-filling ( $n=1$ ), *e.g.* T. Yoshioka, A. Koga, and N. Kawakami, *J. Phys. Soc. Jpn.* **77**, 104702 (2008).  
<sup>10</sup> M. J. Harris, S. T. Bramwell, D. F. McMorrow, T. Zeiske, and K. W. Godfrey, *Phys. Rev. Lett.* **79**, 2554 (1997).

- <sup>11</sup> H. Ueda, H. A. Katori, H. Mitamura, T. Goto, and H. Takagi, Phys. Rev. Lett. **94**, 047202 (2005); D. L. Bergman, R. Shindou, G. A. Fiete, and L. Balents, Phys. Rev. Lett. **96**, 097207 (2006).
- <sup>12</sup> A. S. Wills, R. Ballou, and C. Lacroix, Phys. Rev. B **66**, 144407 (2002).
- <sup>13</sup> P. Fulde, K. Penc, and N. Shannon, Ann.Phys. **11**, 892 (2002); F. Pollmann, P. Fulde, and E. Runge, Phys. Rev. B **73**, 125121 (2006).
- <sup>14</sup> For a review, see chapters of M. J. P. Gingras, and R. Moessner and K. S. Raman, *Highly Frustrated Magnetism*, Eds. C. Lacroix, P. Mendels, F. Mila. Springer Verlag (2010).
- <sup>15</sup> A. Ralko, F. Trouselet, and D. Poilblanc, Phys. Rev. Lett. **104**, 127203 (2010).
- <sup>16</sup> A. Jagannathan, R. Moessner and S. Wessel, Phys. Rev. B **74**, 184410 (2006).
- <sup>17</sup> E. Ressouche, V. Simonet, B. Canals, M. Gospodinov, and V. Skumryev, Phys. Rev. Lett. **103**, 267204 (2009).
- <sup>18</sup> V. Simonet, *private communication*.
- <sup>19</sup> K. S. Raman, R. Moessner, and S. L. Sondhi, Phys. Rev. B **72**, 064413 (2005).
- <sup>20</sup> V. W. Scarola, E. Demler, and S. Das Sarma, Phys. Rev. A **73**, 051601(R) (2006).
- <sup>21</sup> I. Titvinidze, M. Snoek, and W. Hofstetter, Phys. Rev. Lett. **100**, 100401 (2008).
- <sup>22</sup> F. Hébert, G. G. Batrouni, X. Roy, and V. G. Rousseau, Phys. Rev. B **78**, 184505 (2008).
- <sup>23</sup> J. M. Kosterlitz and D. J. Thouless, J. Phys. C **6**, 1181 (1973); J. M. Kosterlitz, J. Phys. C **7**, 1046 (1974).
- <sup>24</sup> A *cairo* spin-1/2 Heisenberg model is currently being studied by I. Rousochatzakis, A. Läuchli, and R. Moessner. A similar 1/3-*ferrimagnetic* phase is discussed. *Private comm.*
- <sup>25</sup> M. Oshikawa and I. Affleck, Phys. Rev. Lett. **79**, 2883 (1997).
- <sup>26</sup> J. Z. Lou, C. Chen, X. Wang, T. Xiang, Z. Su, and L. Yu, Phys. Rev. Lett. **94**, 217207 (2005); B. Xi, S. Hu, J. Zhao, G. Su, B. Normand, X. Wang, arXiv:1106.4605 (2011).
- <sup>27</sup> E. Zhao and A. Paramekanti, Phys. Rev. B **76**, 195101 (2007).
- <sup>28</sup> A. W. Sandvik, Phys. Rev. B **59**, R14157 (1999).
- <sup>29</sup> S. R. Hassan, L. de Medici, and A.-M. S. Tremblay, Phys. Rev. B **76**, 144420 (2007).
- <sup>30</sup> H. Kuroyanagi, M. Tsikamoto, and M. Tsubota, J. Phys. Soc. Jpn. **80**, 034603 (2011); N. Laflorencie and F. Mila, Phys. Rev. Lett. **99**, 027202 (2007).
- <sup>31</sup> K.-K. Ng, Phys. Rev. B **81**, 094426 (2010).
- <sup>32</sup> No Bragg peak is observed in the structure factor on the Bravais lattice (6-site unit cell).
- <sup>33</sup> D. S. Rokhsar and S. A. Kivelson, Phys. Rev. Lett. **61**, 2376 (1988).
- <sup>34</sup> A. Ralko, M. Mambrini, and D. Poilblanc, Phys. Rev. B **80**, 184427 (2009).
- <sup>35</sup> O. F. Syljuasen and S. Chakravarty, Phys. Rev. Lett. **96**, 147004 (2006); O. Cépas and A. Ralko, Phys. Rev. B **84**, 020413(R) (2011).